Angular scanning and variable wavelength surface plasmon resonance allowing free sensor surface selection for optimum material- and bio-sensing

Lakayan, Dina; Tuppurainen, Jussipekka; Albers, Martin; van Lint, Matthijs J.; van Iperen, Dick J.; Weda, Jelmer J.A.; Kuncova-Kallio, Johana; Somsen, Govert W.; Kool, Jeroen

published in
Sensors and Actuators, B: Chemical
2018

DOI (link to publisher)
10.1016/j.snb.2017.12.131

document version
Publisher's PDF, also known as Version of record

Sensors and Actuators B 259 (2018) 972–979

Contents lists available at ScienceDirect

Sensors and Actuators B: Chemical

journal homepage: www.elsevier.com/locate/snb

Angular scanning and variable wavelength surface plasmon resonance allowing free sensor surface selection for optimum material- and bio-sensing

Dina Lakayan[a,b], Jussipekka Tuppurainen[c,d], Martin Albers[c,d], Matthijs J. van Lint[e], Dick J. van Iperen[f], Jelmer J.A. Weda[g], Johana Kuncova-Kallio[c,d], Govert W. Somsen[a], Jeroen Kool[a,*]

[a] Division of Bioanalytical Chemistry, Department of Chemistry and Pharmaceutical Sciences, Faculty of Sciences, Vrije Universiteit, De Boelelaan 1085, 1081 HV Amsterdam, The Netherlands
[b] TI-COAST, Science Park 904, 1098 XH Amsterdam, The Netherlands
[c] BioNavis Ltd., Hermiankatu 6-8 H, 33720 Tampere, Finland
[d] Technex B.V., Industrieweg 35, 1521 NE Wormerveer, The Netherlands
[e] Division of Organic Chemistry, Department of Chemistry & Pharmaceutical Sciences and Amsterdam Institute for Molecules, Medicines and Systems (AIMMS), Vrije Universiteit, De Boelelaan 1083, 1081 HV Amsterdam, The Netherlands
[f] Fine Mechanical Instrumentation and Engineering Group, Faculty of Sciences, Vrije Universiteit, De Boelelaan 1085, 1081 HV Amsterdam, The Netherlands
[g] LaserLaB Amsterdam, Vrije Universiteit, De Boelelaan 1081, 1081 HV Amsterdam, The Netherlands

ARTICLE INFO

Article history:
Received 17 August 2017
Received in revised form
19 December 2017
Accepted 20 December 2017
Available online 21 December 2017

Keywords:
Surface plasmon resonance
Variable wavelength
Angle scanning
Sensor materials
Antibody assay

ABSTRACT

A variable-wavelength Kretschmann configuration surface plasmon resonance (SPR) apparatus with angle scanning is presented. The setup provides the possibility of selecting the optimum wavelength with respect to the properties of the metal layer of the sensorchip, sample matrix, and biomolecular interaction of interest. Monitoring SPR curves over a wide angular range (39°) permits simultaneous determination of the total internal reflection angle (TIR), the resonance angle, and the intensity and width of the SPR dip, which are essential parameters for measuring binding events and achieving optimum sensitivity. The new apparatus was evaluated by recording full SPR curves at different wavelengths ranging from 600 to 890 nm using sensor surfaces of silver, gold and gold with deposited silicon oxide, aluminum oxide, titanium oxide and indium tin oxide which were exposed to air and an aqueous solution of sodium chloride. Clear wavelength dependencies of sensor-material resonance angles and SPR-dip widths were demonstrated. In order to investigate the capability of the system to probe molecular binding to different sensor surfaces, the layer-by-layer adsorption of charged polyelectrolytes was monitored in angular scanning mode at 600, 670, 785, and 890 nm. Although at longer wavelengths lower angular shifts were observed as result of layer deposition, the sharper dip, wider detection window and better signal-to-noise ratios at these wavelengths can be beneficial for binding studies. The applicability for biosensing was tested by immobilizing human serum albumin (HSA) on an aluminum-oxide-coated gold sensor using a new procedure and measuring the binding of anti-HSA antibodies at the optimal wavelength (890 nm) in angular-scanning and fixed-angle mode. The HSA biosensor showed negligible non-specific interaction and yielded almost ten times better sensitivity than obtained with a conventional gold-dextran-based sensor operated at 670/785 nm. Analysis of anti-HSA samples pre-incubated with different concentrations of HSA allowed measurement of the IC50 value. The reported data demonstrate the usefulness of the presented variable-wavelength angle-scanning SPR instrument, permitting continuous recording of full SPR curves in time at any selected wavelength in the 600–890 nm range using a sensor material of choice.

1. Introduction

Surface plasmon resonance (SPR) is a fast optical technique allowing the sensitive detection of refractive index changes at the very near vicinity (within 200 nm) of a thin metal layer [1]. Most

* Corresponding author.
E-mail address: j.kool@vu.nl (J. Kool).

https://doi.org/10.1016/j.snb.2017.12.131
0925-4005/

commercially available SPR systems utilize a Kretschmann configuration, which basically comprises a prism with a thin metal film on the bottom side. When a plane-polarized light beam propagates in the prism, at an incident angle larger than the critical angle, total internal reflection (TIR) will occur and an evanescent wave (EW) is formed. Depending on the incident angle, the EW can excite delocalized electrons in the metal layer causing SPR and a decrease of the intensity of reflected light is observed. The resonance angle at which the reflected intensity is minimal is sensitive to the refractive index of the medium close to the metal side, but also depends on the wavelength of the incident light and the metal characteristics. Thin gold and silver films of about 50 nm are frequently used materials to generate SPs [2]. Other materials that support SP waves include aluminum, copper, palladium, cobalt, nickel, vanadium, chromium, tungsten and some semiconductors [3].

The most commonly used SPR system, BIAcore, uses the light of a 633 nm or 760-nm He-Ne laser focused onto the sensorchip [4]. The reflected light is monitored by an array detector allowing continuous determination of the resonance angle. Plotting the shift of the resonance angle against time in a sensorgram indicates local refractive index changes caused by the probed medium [5–8]. With a multi-parametric SPR instrument (Bionavis) the intensity of the reflected laser light is detected in fast angular-scan mode (scan speed: $8^\circ\ s^{-1}$) in real time. This setup continuously provides full SPR curves (intensity vs. incident angle) over a 39° wide range, and thus allows detailed monitoring of changes in the position (resonance angle), shape, width and intensity of the SPR curve. The wide-angle range also permits measurements on different sensor metals and inorganic materials deposited on gold exposed to both gaseous and liquid media. Two laser sources (670 and 785 nm) are available for SPR measurements using this system [9–11].

In order to achieve optimum SPR performance and sensitivity with various sensor materials and types of samples, the possibility to freely select light of the appropriate wavelength would be advantageous. Using a Kretschmann configuration, Homola et al. reported on the real-time monitoring of the intensity of reflected light as a function of wavelength instead of incident angle [12,13]. The light of a halogen source (550–950 nm) was applied at a fixed angle and a spectral analyzer was used to determine the wavelength of minimum reflection [13]. Using a similar setup, Eum et al. obtained a more sensitive detection of small molecules as compared to conventional SPR [14]. Nelson and co-workers used low power diode and He-Ne laser sources to measure the film thickness in the near-infrared range (NIR) at 814 and 1152 nm. They reported that at these longer wavelengths the SPR curves were sharpened greatly as compared to 632.8 nm, and despite doubling of the excitation wavelength, no loss in sensitivity in the film thickness measurement was observed allowing measurement of thicker films. Using NIR also simplifies the SPR measurements for molecules with absorption bands in the visible region [15]. So far, most of the reported SPR studies employing variable wavelengths were concerned with optimizing the thickness of the sensor metal film for specific analyses [15–22]. An SPR report on the use of sensors of gold and silicon oxide deposited on gold in combination with two wavelengths from a He-Ne laser (623.8 and 545.0 nm) emphasized the effect of wavelength on the Q-factor, which represents the confinement of plasmons and thus the width of the intensity dip in the SPR curve [23].

We combined a white light source and monochromator from a spectrophotometer with a multi-parametric SPR device to enable real-time incident angle scanning (39–78 degrees) at wavelengths ranging from 500 to 890 nm (Fig. 1). The new instrument was evaluated by studying the effect of the wavelength on SPR curves obtained for different sensor materials exposed to both air and aqueous media. Probing of molecular adsorption/binding was tested by deposition of polyelectrolyte multilayers on different sensors, while assessing the SPR curve shape, resonance angle shift, signal-to-noise ratio, sensitivity and angular detection window at several wavelengths. Biosensing capabilities of the SPR system were investigated by producing human serum albumin (HSA)-immobilized sensors and measuring the binding of polyclonal anti-HSA antibodies to the SPR sensorchips. For the HSA protein immobilization, a derivatization chemistry on an aluminum oxide coated gold sensor was used.

2. Materials and methods

2.1. Chemicals and reagents

Sodium chloride, poly sodium 4-styrenesulfonate (PSS), polyallylamine hydrochloride (PAH), polyethylenimine (PEI), lysozyme, human serum albumin (HSA), sulfuric acid, hydrogen peroxide, ethanol (anhydrous), (3-aminopropyl) triethoxysilane (APTES), dry acetonitrile, triethyamine (TEA), carbonyldiimidazole (CDI), sodium borate, sodium hydroxide solution 50% in water, ethanolamine hydrochloride, hellmanex cleaning solution, phosphate buffered saline (PBS) and anti-human albumin antibody produced in rabbit (whole antiserum) were purchased from Sigma-Aldrich (Steinheim, Germany). Acetone was from Biosolve B.V. (Valkenswaard, the Netherlands) or J.T. Baker (Deventer, the Netherlands). HPLC grade water was produced by a Milli-Q purification system from Millipore (Amsterdam, the Netherlands).

2.2. Variable-wavelength SPR instrument

An SPR setup allowing wavelength selection (500–890 nm) and real-time angle scanning (39-78°) was constructed by combining the excitation module of an FP-1520 fluorescence detector of Jasco (Ijsselstein, the Netherlands) with a multi-parametric MP-SPR Navi 210A instrument of BioNavis (Tampere, Finland) (Fig. 1). An XBO Xenon lamp (150W/1OFR) of OSRAM (Munich, Germany) was used as a light source from which the wavelength for SPR measurement was selected using the excitation monochromator with the spectral bandwidth fixed at 18 nm. The light was directed outside the detector via a plane mirror mounted on the position of the cuvette holder and then transferred to the SPR instrument using an F240FC-780 package of Thorlabs (Dachau/Munich, Germany) comprising a 50-μm multimode optical fiber and two dedicated lenses. The light leaving the fiber is led through an LPVISE2 × 2 polarizer of Thorlabs onto the triangular 60° prism facing the sensor surface. The intensity of the reflected light was measured with the standard photodetector housed in the Bionavis system. Commercially available Bionavis MP-SPR Navi Control software was slightly modified (version 3.0.2) and used for data collection.

2.3. Sensor materials, surface modifications and SPR analyses

2.3.1. Sensor materials

The sensors used in this study were purchased from BioNavis (Tampere, Finland). Ion-beam assisted evaporation [24] was used to deposit the metals on 0.55-mm glass soda lime substrate, with 2-nm chromium as an adhesion layer. In addition to one-line quartz crystal microbalance as a standard quality control tool for the evaporation deposition process, a BioNavis SPR-Navi instrument and optical modelling of the SPR data was used for defining the thickness of the metal layers [25,26]. Metal oxide sensors were manufactured using an accurate atomic layer deposition (ALD) process [27]. No additional thickness verification steps were made for the metal oxide layers. The following SPR sensor materials with indicated thicknesses from BioNavis were used: gold (48 nm), silver (50 nm), and 50-nm gold with, respectively, 12 nm silicon oxide, 5 nm aluminum oxide, 5 nm titanium oxide or 10 nm indium tin

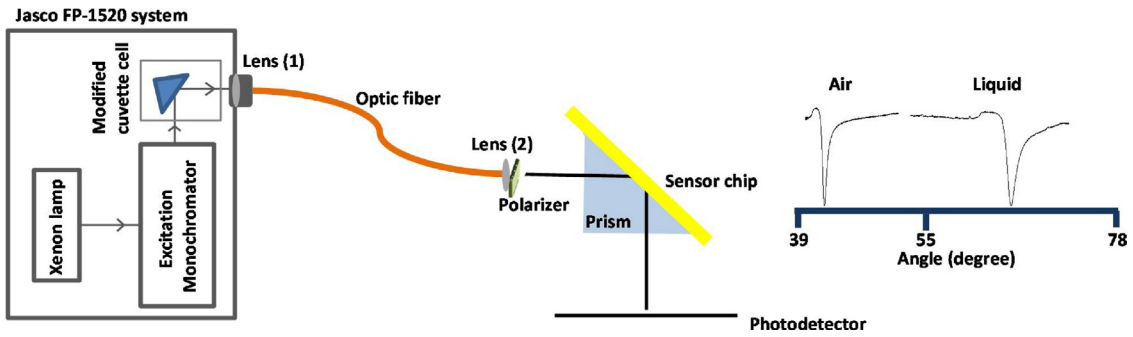

Fig. 1. Schematic view of the variable wavelength SPR setup with angular scanning allowing the recording of full SPR curves in real time at any selected wavelength ranging from 500 to 890 nm. The SPR curves in air and in liquid media appear at angles lower and higher than 55 °, respectively, as demonstrated in the figure for 670 nm.

oxide. For the adhesion of the oxides on the gold surface, a 2-nm layer of chrome was used. Full SPR curves (angular range, 39-78°) were recorded at 500, 550, 600, 650, 670, 700, 750, 785, 800, 850 and 890 nm for all sensor materials exposed to both air and to 0.15 M sodium chloride in water.

2.3.2. Sensors with polyelectrolyte layers

The sequential adsorption of polyelectrolytes on the various sensor materials was monitored at 600, 670, 785 and 890 nm. The liquid flow rate over the sensor chip was set at 50 μL/min allowing efficient polyelectrolyte adsorption and the flow cell was kept at 20 °C. Before applying the polyelectrolyte layers, the sensor surfaces were cleaned twice with 5% Hellmanex solution for 4 min and then equilibrated with 0.15 M sodium chloride (running electrolyte) until a stable baseline was obtained. Subsequently, polyelectrolyte layers were applied by successively flushing solutions of 0.1 mg/ml PEI, PSS, PAH, PSS and PAH in running electrolyte for 4 min each while monitoring the SPR signal at one specific wavelength. Next, solutions of lysozyme and HSA (both 1 mg/ml) in running electrolyte were successively flushed over the five-polyelectrolyte layer for 4 min while measuring the SPR output. Sensorgrams (SPR resonance angle shift vs. time) were recorded for each tested wavelength and sensor material. Sensor surfaces were regenerated by flushing with 1% Hellmanex solution for 4 min.

2.3.3. Aluminum oxide sensor with immobilized HSA

HSA was immobilized covalently onto an aluminum oxide sensor surface according to a reported method for immobilization of enzymes on a nanoporous aluminum oxide (NAO) [28]. NAO is a self-organized material easily manufactured by anodization of thin aluminum foils. The aluminum oxide surface was first hydroxylated offline by exposure to a mixture of 30% hydrogen peroxide and concentrated sulfuric acid (1:3, v/v) for 5 min, rinsed with water and ethanol, and then stored in anhydrous ethanol. The surface wettability was determined by contact angle measurements done in a similar way as W.J. Kim et al. [29].

Next, the surface was silanized by immersion in 10 mL dry acetonitrile containing 200 μL APTES in a 50-mL round bottom flask for 1 h. After subsequent addition of 200 μL trimethylamine, the sensor was incubated for 2 h at 25 °C while shaking at 200 rpm and then taken out of the solution and dried under a stream of air. Subsequently, the sensor was heated at 120 °C for 30 min and the surface was successively washed with ethanol, water and acetone, and then dried at 120 °C for 1 h. In the next step, the amino groups on the sensor surface were activated with 0.5 g CDI and 200 μL trimethylamine in 5 mL acetonitrile for 1 h at 25 °C, while shaking at 200 rpm. The surface was successively washed with ethanol, water and acetone, and thoroughly dried at 120 °C for 30 min. The activated surface was then exposed to a solution of HSA in 25 mM borate (pH 9) for 20–24 h at room temperature. Finally, the surface was rinsed with PBS and deactivated with 1 M ethanolamine hydrochloride (pH 8.5) for 1 h at room temperature, and again rinsed with PBS. The binding of anti-HSA to the HSA-immobilized aluminum oxide sensor was monitored using the new SPR setup at 890 nm using both angular-scan and fixed-angle mode. The SPR flow rate was 30 μL/min in order to allow good protein–protein interaction and the sensor cell was thermostated at 20 °C. Anti-HSA was analysed in the concentration range of 0.1–100 μg/ml, in duplicate, for 7 min per concentration tested. After each analysis, the sensor surface was regenerated (for removing bound anti-HSA) by flushing with 50 mM sodium hydroxide for 1 min. Kinetic constants were calculated using TraceDrawer software (version 1.7; Ridgeview Instruments, Vange, Sweden). Affinity curves were plotted using GraphPad PRISM Software (San Diego, CA, USA).

3. Results and discussion

The overall performance of the new SPR system was studied by (i) evaluating the SPR properties of different sensor materials as function of wavelength, (ii) investigating molecular binding on different sensor surfaces at different wavelengths using polyelectrolytes as test compounds, and (iii) demonstrating applicability through a model assay probing antibody-protein interactions employing a new aluminum-oxide-based sensor in combination with a wavelength of 890 nm.

3.1. SPR curves for different sensor materials at variable wavelength

In order to investigate the potential of the new system, full SPR curves were recorded at 11 selected wavelengths for six different sensor materials exposed to both air and an electrolyte solution (Fig. 2). The TIR, the intensity and width of the SPR dip (i.e. the negative peak in the SPR curve), and the resonance angles were determined. The tested sensor materials were gold, silver, and silicon oxide, aluminum oxide, titanium oxide and indium tin oxide deposited on gold. The tested wavelengths were between 500 and 890 nm (from 500 nm in 50 nm increments), also including 670 and 785 nm since these are employed in the original multi-parametric SPR instrument. The TIR angle predominantly depends on the difference in refractive index of the prism material and the probed medium. For all tested wavelengths, the TIR angle of the different sensor materials evaluated was 41.3 ± 0.1 ° and 61.2 ± 0.1 ° when exposed to air and electrolyte solution, respectively. Hence, the TIR angle indeed was virtually independent on wavelength. When exposed to air, for all sensor materials the SPR curves were observed below an incident angle of 55°, whereas for the liquid samples the curves were positioned above 55 ° (Fig. 2). At 500 and 550 nm, no SPR curves were observed. Indeed, for gold at wavelengths shorter than 520 nm the plasmons are not excited, precluding SPR [30].

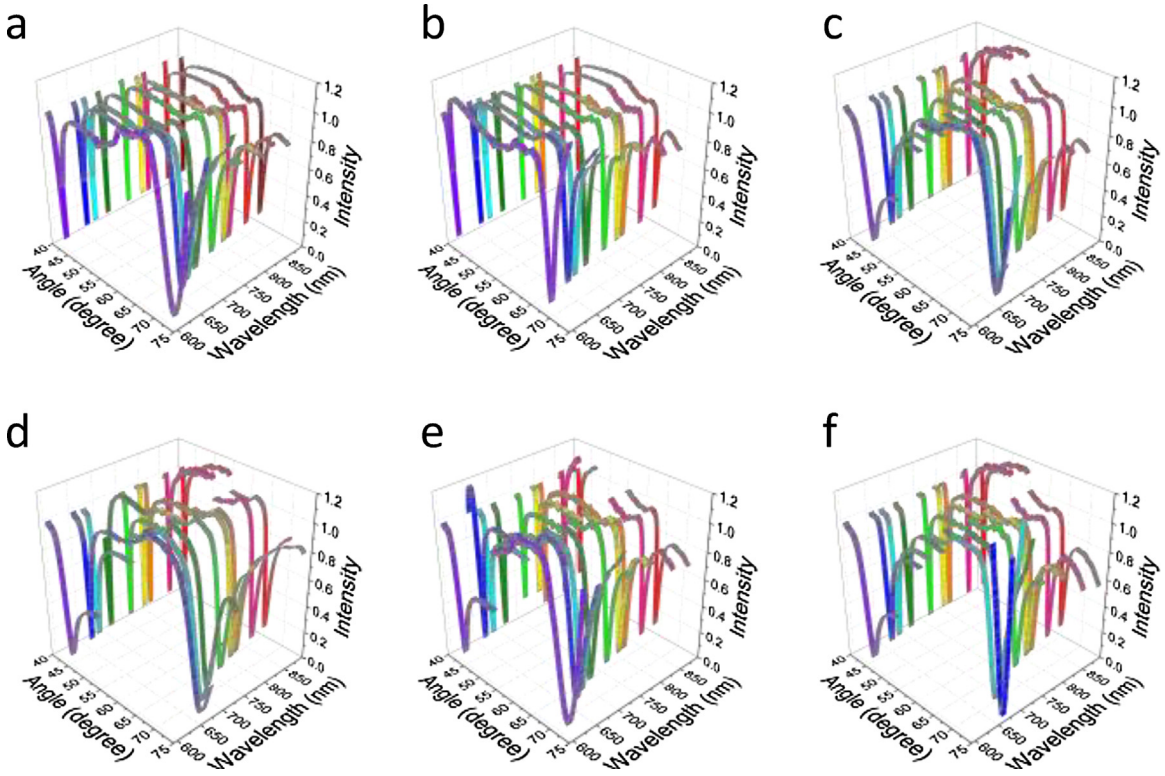

Fig. 2. SPR curves for the sensor materials gold (a), silver (b), aluminum oxide (c), indium tin oxide (d), silicon oxide (e), and titanium oxide exposed to air (39-55°) and to NaCl pH 9 electrolyte solution (55-78°) recorded at 600, 650, 670, 700, 750, 785, 800, 850 and 890 nm.

Moreover, for incident light with wavelengths shorter than 630 nm, the resonance angle observed for the liquid samples may occur outside the angular range covered by the instrument (upper limit, 78°).

The experimentally obtained SPR curves at 600–890 nm using gold as sensor material are depicted in the supporting information in Fig. S1a. The full-width at half minimum (FWHM) of the SPR dips showed a wavelength dependency. The FWHM in the experimental SPR curves decreased with longer wavelengths of the incident light (Fig. S2), which is in correspondence with theoretical calculations. The sensor materials showed a decrease in FWHM for the NIR wavelengths (750–890 nm) when compared to the visible range (600–700 nm). The narrower SPR curves can be explained by the lower attenuation of the surface plasmon wave at longer wavelengths [21]. A sharper SPR dip allows more accurate determination of the resonance angle. Other potential advantages of using NIR light for SPR measurements is that it is less likely to be absorbed by probed molecules [15,31] and it penetrates deeper into the sample than light of shorter wavelengths [32].

From the SPR curves recorded for the sensor materials exposed to air and electrolyte solution, the resonance angles were measured as a function of wavelength. All materials showed a decrease of resonance angle with increasing wavelength (see supporting information Fig. S3). The angle decline was most pronounced in the visible range (600–750 nm) and gradually lessened in the NIR region to reach a plateau. However, the absolute resonance angle values and the decline was significantly different for the respective materials. For instance, when exposed to the liquid sample, the resonance angles for silver and aluminum oxide at 600 nm were 69.5 and 77.5°, respectively, which decreased to 63.5 (-6.0) and 67.5 (-10.0) degrees, respectively, at 890 nm. The variation in resonance angle among the sensor materials was the largest at shorter wavelength, ranging respectively between 42 and 47.5° and between 64 and 78° for air and liquid samples at 600 nm. For some materials, such as titanium oxide and aluminum oxide, the resonance angles at 600 nm are relatively close to the upper limit of the instrument, which restricts the dynamic angular range for sample measurements and prohibits recording of full SPR curves. At long wavelength (890 nm) the resonance angles of the tested materials were in the much smaller range of 42–44 and 64–67° for air and liquid, respectively. As adsorption or binding to the sensor surface leads to a shift of the resonance angle to larger values, the relatively low resonance angles as observed for the sensor materials at long wavelengths, in principle provides the instrument with a larger dynamic angular range. In other words, the option to use the incident light of e.g. 890 nm yields the possibility to cover a larger range of refractive index changes induced by samples. Still, the magnitude of the resonance angle is also wavelength dependent and should be taken into account as well (see Section 3.2).

The SPR curves recorded at 670 and 785 nm for the gold sensor material exposed to the electrolyte solution with the new instrument were compared with curves obtained using the standard laser sources of the multi-parametric SPR instrument (Fig. S1b). The curves obtained with the variable wavelength setup showed very similar to the conventionally recorded SPR curves. The relative dip intensities and widths were similar. Based on SPR theory (see Supporting information), the theoretical SPR curves were calculated for the sensor materials at different wavelengths (shown for gold in Fig. S4). The experimental curves correlated well with the theoretical ones, taking into account that the optical constants of thin gold layers are usually somewhat different than those from the bulk values. [28] Overall, these results demonstrate that the setup with the Xenon source and monochromator reliably allows measurement of full SPR curves at any wavelength between 600 and 890 nm.

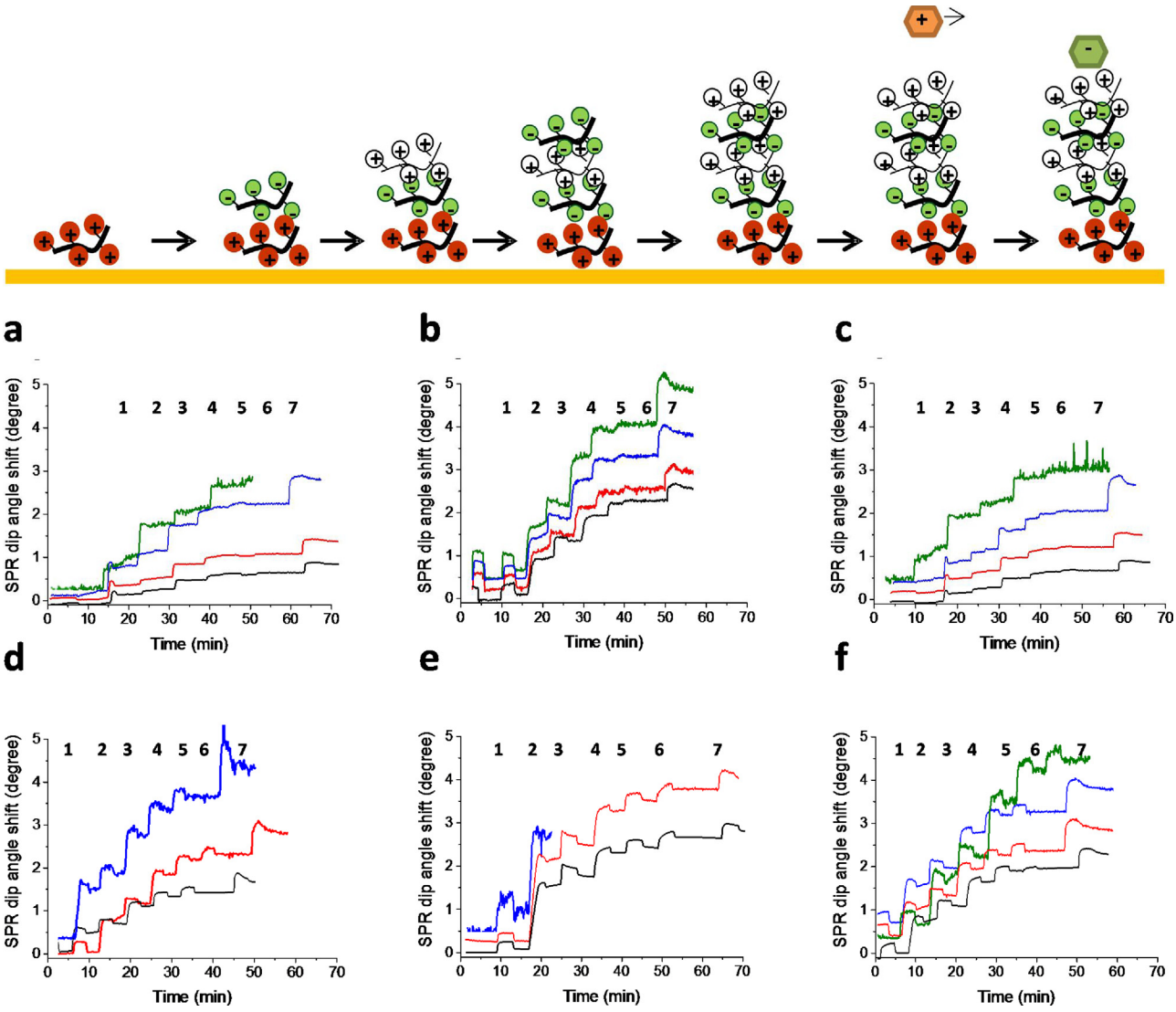

Fig. 3. Top: Schematic view of the successive layer-by-layer adsorption of the polyelectrolytes PEI, PSS, PAH, PSS and PAH, respectively, to a sensor surface, followed by exposure to lysozyme and then to HSA. Bottom: SPR sensorgrams recorded at 600 (green), 670 (blue), 785 (red) and 890 (black) nm during the layer-by-layer adsorption of the polyelectrolytes to the sensor surfaces of (a) gold, (b) silver, (c) aluminum oxide, (d) indium tin oxide, (e) silicon oxide, and (f) titanium oxide. (For interpretation of the references to colour in this figure legend, the reader is referred to the web version of this article.)

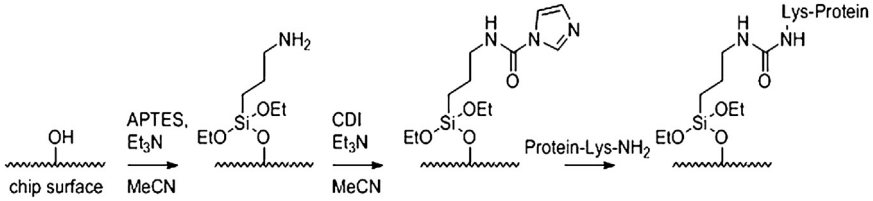

Fig. 4. Chemistry of immobilization procedure (i.e. covalent derivatization) of HSA protein on the aluminum oxide sensor chip.

3.2. Probing polyelectrolyte adsorption on different sensor materials by variable-wavelength SPR

In order to evaluate the SPR response upon molecular binding to the different sensor surfaces as a function of wavelength, the adsorption of multiply-charged polymers (polyelectrolytes) was monitored. Oppositely charged polymers, such as the positive polycations PEI and PAH, and the negative polyanion PSS, can provide a convenient means to adhere successive molecular layers to sensor surface materials in a controlled fashion. Strong electrostatic interaction allows the formation of multiple polymer layers of alternating charge. Solutions of PEI, PSS and PAH in 0.15 M sodium chloride were subsequently flushed over the six tested sensor materials (schematically depicted at the top of Fig. 3), while recording the SPR signal in angular scanning mode at 600, 670, 785, and 890 nm. After applying five layers of charged polymers (ending with PAH), solutions of lysozyme (pI 11.1) and HSA (pI, 4.7) [33] were subsequently injected. From these data, sensorgrams (resonance angle shift vs. time) were constructed (Fig. 3a–f). The stepwise adsorption of the polyelectrolytes was clearly monitored by SPR. For all sensor materials, larger resonance angle shifts were observed per layer when using the light of shorter wavelength. As

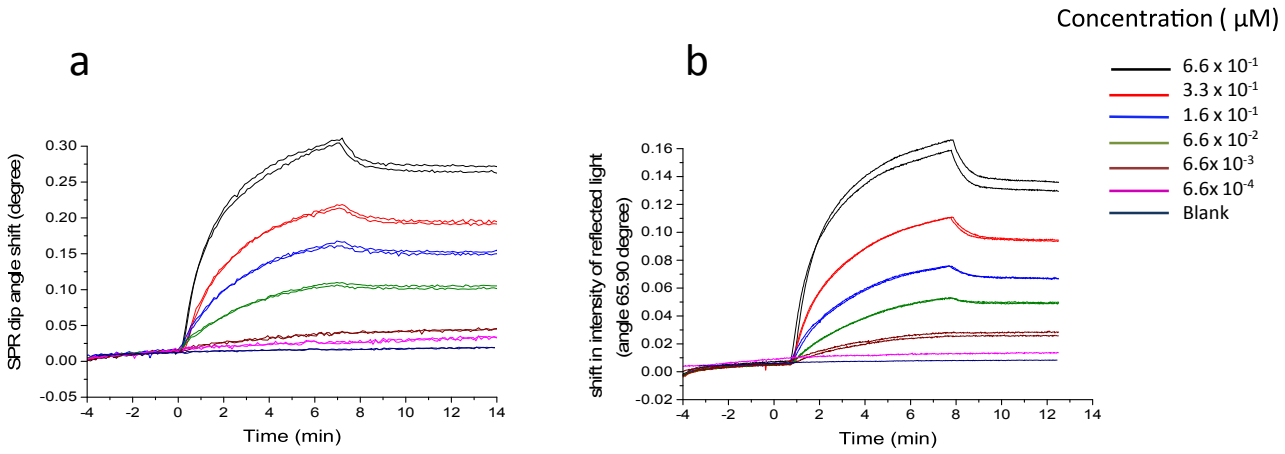

Fig. 5. Sensorgrams constructed from SPR analyses at 890 nm of different concentrations of anti-HSA (0–100 μg/ml) using (a) angular-scan mode and (b) fixed-angle mode (65.90°) employing a HSA-aluminum oxide sensor chip.

the resonance angle is larger at a shorter wavelength (see Section 3.1), the resonance angle occurs relatively close to the upper limit of the instrument and therefore measuring angle shifts might be limited. This was most pronounced for the sensor materials gold, silicon oxide and titanium oxide. Larger resonance shifts mean higher SPR responses per amount of adsorbed material, which seems favorable. However, as can be observed in Fig. 3, the level of noise also was highest when using the shortest tested wavelength of 600 nm. Therefore, from the sensorgrams signal-to-noise ratios (S/Ns) were determined for the signals obtained after adsorption of the fifth layer (PAH) (see Supporting information Fig. S6). It was found that for most sensor materials optimum S/Ns were obtained at longer wavelengths (785 and 890 nm). The narrower dip widths observed at longer wavelengths apparently lead to a more precise (i.e. less noisy) determination of the resonance angle shift. Silver, however, showed similar S/N values for all tested wavelengths. In conclusion, although at longer wavelengths lower angular shifts are observed as result of layer deposition, the sharper peaks (and thus higher S/N ratios) and also their wider detection window can be beneficial for studying the binding of high-molecular-weight analytes to the sensor surfaces. Multi-wavelength SPR detection in principle also would allow calculation of the thickness of each adsorbed layer, as previously shown for a polyelectrolyte adsorption study employing three wavelengths [26].

Upon injection of lysozyme, no shift of de resonance angle was observed for all tested sensor materials and wavelengths. This was expected as the fifth layer of PAH is strongly positively charged, preventing adsorption of the positively charged basic lysozyme by electrostatic repulsion. In contrast, the overall negatively charged HSA showed significant adsorption to the PAH layer as indicated by the increase of resonance angle for all sensor chip materials tested. This also indicated that at longer wavelengths the sensor materials show good potential for probing protein binding.

3.3. *Probing antibody-protein binding by SPR using an aluminum oxide sensor*

For evaluation of the versatility and performance of the variable wavelength SPR system, HSA was covalently immobilized on an aluminum oxide sensor surface and the binding of anti-HSA was assessed at 890 nm. The new immobilization procedure is depicted in Fig. 4 and described in Section 2.3.3. Briefly, the aluminum oxide surface was hydroxylated. [29] The contact angle tests showed a higher contact angle of the water droplet with the hydroxylated surface (in comparison with the untreated surface) implying the more hydrophobic surface condition due to the presence of oxide groups only (see supporting information, Fig. S7.) After covalent attachment of APTES [28,34–36], the surface was activated with CDI to form aminosilane that allowed coupling of protein (HSA in our case) via its N-terminus and lysine residues.

Serial dilutions of a polyclonal anti-HSA sample (0–666 nM) were analysed with the SPR setup at 890 nm using the aluminum oxide-HSA sensor. Constructed sensorgrams (resonance angle shift vs. time) obtained using angular scan mode clearly indicate reproducible concentration-dependent binding (Fig. 5a). From the data obtained, the association constant $k_a = 5.58E+3\ (M^*s)^{-1}$ and dissociation constant $k_d = 2.51E\text{-}4\ (s^{-1})$ were determined from which the dissociation constant $K_D = 4.30E\text{-}8\ (M)$ was retrieved. Binding could be detected down to concentrations of 0.6 nM of anti-HSA, which is about 10 times more sensitive than reported for SPR measurements of anti-HSA binding to immobilized HSA using traditional Bionavis angular-scanning mode SPR with a conventional carboxymethyl dextran gold sensor. The larger penetration depth of the evanescent wave at 890 nm and the more rigid sensor surface (as compared to the hydrogel) probably add to the higher molar response obtained with the HSA-aluminum oxide sensor.

In order to compare the sensitivity of the SPR system in angle scanning mode and fixed-angle mode, measurements of the same concentrations of anti-HSA (0–666 nM) were repeated in fixed-angle mode. In angular-scan mode, the shift in the SPR dip angle is observed, whereas in fixed-angle mode the change in intensity of the reflected light at a selected angle is measured [37]. For anti-HSA the intensity of the reflected light at an angle of 65.90° was monitored as a function of time (Fig. 5b). The obtained sensorgrams showed less noise than observed in angular-scan mode, but for low anti-HSA concentrations, the absolute signal was lower allowing detection down to 0.6 nM in both cases. Comparative results of angle scanning vs. fixed angle SPR measurements using the here presented system, can be found in the supporting information (Table S1). The constructed binding curves for angular-scan and fixed-angle modes can be found in supporting information as well (Fig. S9). Finally, the suitability of the developed SPR system for affinity assays was investigated by analyzing anti-HSA samples of 50 μg/ml pre-incubated anti-HSA with different concentrations of HSA (0–1000 μg/ml) up to antibody binding saturating conditions. Fitting the data obtained yielded an IC50 value of 11.23± 0.01 nM (see supporting information for details).

In order to study the stability of the immobilized HSA on the sensor surface further, a prepared aluminum oxide-HSA sensor was stored in PBS for one week at 4°C. Then this sensor was used to analyse the same concentrations of the anti-HSA sample in fixed-angle mode at 65.90° (Fig. S8). It was found that results obtained

were very similar to the ones obtained using a freshly prepared sensor (Fig. 5b) showing no loss of binding capacity.

4. Conclusions

This study presents an angle-scanning SPR system with variable wavelength selection. The performance of the system was assessed by measuring full SPR curves (39–78 degrees) of different sensor materials exposed to air and an electrolyte solution at wavelengths between 500 and 890 nm. The obtained data on resonance angle, the width of the SPR dip, and the experimentally derived real and imaginary part of the refractive index, were found to be close to theoretical values. The absolute resonance angle values were significantly different for the respective materials, but all materials showed a decrease of resonance angle with increasing wavelength. The decline was most pronounced in the visible range (600–750 nm). The width of the dip in the SPR curves decreased with a longer wavelength of the incident light. Hence, at longer wavelengths, the largest dynamic range was obtained for measuring refractive index changes caused by analyte adsorption or binding to the sensor surface. For all sensor materials, larger resonance angle shifts were observed upon analyte adsorption when using the light of shorter wavelength. However, at shorter wavelength, the resonance angle shift might be outside the measurable angular range of the instrument. Moreover, at longer wavelengths for most sensor materials optimum S/Ns were obtained and the penetration depth of the evanescent wave into the sample increases. The applicability of SPR system was demonstrated by probing the interaction between anti-HSA and HSA immobilized on an aluminum oxide sensor surface. Specific binding of anti-HSA could be detected down to 0.6 nM.

Conflicts of interest

The authors have declared no conflict of interest.

Acknowledgments

This research is funded by Netherlands Organization for Scientific Research (NWO) in the framework of Technology Area COAST [project number 053.21.107] with Wageningen University, RIKILT, Heineken, Synthon, Technex, EuroProxima, Waterproef as partners and BioNavis and Plasmore as associated partners.

Appendix A. Supplementary data

Supplementary data associated with this article can be found, in the online version, at https://doi.org/10.1016/j.snb.2017.12.131.

References

[1] H.H. Nguyen, J. Park, S. Kang, M. Kim, Surface plasmon resonance: a versatile technique for biosensor applications, Sensors (Basel) 15 (2015) 10481–10510.
[2] J.F. Rusling, Biomolecular Films: Design, Function, and Applications, CRC Press, 2003.
[3] J.E.P. Jones, A.B. Kaye, R.F. Haglund, D.E. Cliffel, D. Wright, Optical sensors including surface modified phase-change materials for detection of chemical, biological and explosive compounds Google Patent s2013.
[4] J.A. Tuszynski, The Emerging Physics of Consciousness, Springer Science & Business Media, 2006.
[5] N.A. Drescher, Surface plasmon resonance (SPR) analysis of binding interactions of proteins in inner-ear sensory epithelia, Methods Mol. Biol. y (Clifton, NJ) 493 (2009) 323–343.
[6] M. Taulés i Marín, J.F. Comas Riu, Overview of Molecular Interactions Using Biacore, Capítol Del Llibre: Handbook of Instrumental Techniques for Materials, Chemical and Biosciences Research, Centres Científics i Tecnològics Universitat de Barcelona, Barcelona, 2012, pp. 10, Part III Biosciences technologies (BT), BT 10.
[7] R.J. Pei, X.Q. Cui, X.R. Yang, E.K. Wang, Amplified immunoassay of human IgG using real-time biomolecular interaction analysis (BIA) technology, Chin. J. Chem. 20 (2002) 441–446.
[8] H.A. Schuessler, A. Mershin, A.A. Kolomenskii, D.V. Nanopoulos, Surface plasmon resonance study of the actin-myosin sarcomeric complex and tubulin dimers, J. Mod. Opt. 50 (2003) 2381–2391.
[9] K. Niegelhell, S. Leimgruber, T. Grießer, C. Brandl, B. Chernev, R. Schennach, et al., Adsorption studies of organophosphonic acids on differently activated gold surfaces, Langmuir 32 (2016) 1550–1559.
[10] T. Mohan, K. Niegelhell, C. Nagaraj, D. Reishofer, S. Spirk, A. Olschewski, et al., Interaction of tissue engineering substrates with serum proteins and its influence on human primary endothelial cells, Biomacromolecules 18 (2017) 413–421.
[11] J. Kuncova-Kallio, A. Jokinen, J.W. Sadowski, N. Granqvist, Characterization of nanolaminate thickness using multi-parametric surface plasmon resonance, 2013 International Conference on Manipulation, Manufacturing and Measurement on the Nanoscale (2013) 259–263.
[12] M. Piliarik, J. Homola, Surface plasmon resonance (SPR) sensors: approaching their limits? Opt. Express 17 (2009) 16505–16517.
[13] J. Homola, H. Vaisocherová, J. Dostálek, M. Piliarik, Multi-analyte surface plasmon resonance biosensing, Methods 37 (2005) 26–36.
[14] N.S. Eum, D.E. Kim, S.H. Yeom, B.H. Kang, K.J. Kim, C.S. Park, et al., Variable wavelength surface plasmon resonance (SPR) in biosensing, Biosystems 98 (2009) 51–55.
[15] B.P. Nelson, A.G. Frutos, J.M. Brockman, R.M. Corn, Near-infrared surface plasmon resonance measurements of ultrathin films. 1. Angle shift and SPR imaging experiments, Anal. Chem. 71 (1999) 3928–3934.
[16] K. Balaa, M. Kanso, S. Cuenot, T. Minea, G. Louarn, Experimental realization and numerical simulation of wavelength-modulated fibre optic sensor based on surface plasmon resonance, Sens. Actuators B 126 (2007) 198–203.
[17] H.R. Gwon, S.H. Lee, Spectral and angular responses of surface plasmon resonance based on the Kretschmann prism configuration, Materi. Trans. 51 (2010) 1150–1155.
[18] G. Xu, M. Tazawa, P. Jin, S. Nakao, K. Yoshimura, Wavelength tuning of surface plasmon resonance using dielectric layers on silver island films, Appl. Phys. Lett. 82 (2003) 3811–3813.
[19] G. Xu, M. Tazawa, P. Jin, S. Nakao, Surface plasmon resonance of sputtered Ag films: substrate and mass thickness dependence, Appl. Phys. A 80 (2005) 1535–1540.
[20] M. Iga, A. Seki, K. Watanabe, Gold thickness dependence of SPR-based hetero-core structured optical fiber sensor, Sens. Actuators B 106 (2005) 363–368.
[21] J. Homola, I. Koudela, S.S. Yee, Surface plasmon resonance sensors based on diffraction gratings and prism couplers: sensitivity comparison, Sens. Actuators B 54 (1999) 16–24.
[22] K. Johansen, H. Arwin, I. Lundström, B. Liedberg, Imaging surface plasmon resonance sensor based on multiple wavelengths: sensitivity considerations, Rev. Sci. Instrum. 71 (2000) 3530–3538.
[23] W. Mukhtar, P.S. Menon, S. Shaari, M. Malek, A. Abdullah, Angle shifting in surface plasmon resonance: experimental and theoretical verification, J. Phys.: Conf. Ser. (2013) 012028 (IOP Publishing).
[24] J.K. Hirvonen, Ion beam assisted thin film deposition, Mater. Sci. Rep. 6 (1991) 215–274.
[25] H. Jussila, H. Yang, N. Granqvist, Z. Sun, Surface plasmon resonance for characterization of large-area atomic-layer graphene film, Optica 3 (2016) 151–158.
[26] N. Granqvist, H. Liang, T. Laurila, J. Sadowski, M. Yliperttula, T. Viitala, Characterizing ultrathin and thick organic layers by surface plasmon resonance three-wavelength and waveguide mode analysis, Langmuir 29 (2013) 8561–8571.
[27] M. Leskelä, M. Ritala, Atomic layer deposition (ALD): from precursors to thin film structures, Thin Solid Films 409 (2002) 138–146.
[28] M. Kjellander, Nanoporous Aluminum Oxide–A Promising Support for Modular Enzyme Reactors, 2013.
[29] W.J. Kim, S. Kim, B.S. Lee, A. Kim, C.S. Ah, C. Huh, et al., Enhanced protein immobilization efficiency on a TiO2 surface modified with a hydroxyl functional group, Langmuir 25 (2009) 11692–11697.
[30] B.H. Ong, X. Yuan, S.C. Tjin, J. Zhang, H.M. Ng, Optimised film thickness for maximum evanescent field enhancement of a bimetallic film surface plasmon resonance biosensor, Sens. Actuators B 114 (2006) 1028–1034.
[31] J.F. Glickman, Assay Development for Protein Kinase Enzymes, 2012.
[32] R. Ziblat, V. Lirtsman, D. Davidov, B. Aroeti, Infrared surface plasmon resonance: a novel tool for real time sensing of variations in living cells, Biophys. J. 90 (2006) 2592–2599.
[33] P.-R. Yeh, W.-L. Tseng, Human serum albumin-coated gold nanoparticles for selective extraction of lysozyme from real-world samples prior to capillary electrophoresis, J. Chromatogr. A 1268 (2012) 166–172.
[34] A.V. Williams, A. Davydov, S.G. Motayed, P. Sundaresan, et al., Immobilization of streptavidin on 4H–SiC for biosensor development, Appl. Surf. Sci. 258 (2012) 6056–6063.
[35] Z.-H. Wang, G. Jin, Covalent immobilization of proteins for the biosensor based on imaging ellipsometry, J. Immunol. Methods 285 (2004) 237–243.
[36] H.J. Lee, D. Nedelkov, R.M. Corn, Surface plasmon resonance imaging measurements of antibody arrays for the multiplexed detection of low molecular weight protein biomarkers, Anal. Chem. 78 (2006) 6504–6510.

[37] J.B. Beusink, A.M. Lokate, G.A. Besselink, G.J. Pruijn, R.B. Schasfoort, Angle-scanning SPR imaging for detection of biomolecular interactions on microarrays, Biosens. Bioelectron. 23 (2008) 839–844.

Biographies

Dina Lakayan (MSc.) obtained her Master's degree in Analytical Chemistry from Stockholm University (Sweden) in 2012. She has performed her Ph.D. at Division of Bioanalytical Chemistry, Vrije Universiteit Amsterdam (the Netherlands). This work was funded by Netherlands Organization for Scientific Research (NWO) in the framework of Technology Area COAST. Her Ph.D. research focused on hardware (variable wavelength, multiplexing) innovation of Surface Plasmon Resonance and method development for affinity profiling of biopharmaceutical by coupled liquid chromatography-Surface Plasmon Resonance biosensing.

Jussi Tuppurainen (44) has joined BioNavis Ltd in 2007 and is working as a Technical Director. He received his MSc degree in physics from University of Jyväskylä in 1998. Between 1999 and 2007 he has worked in Technical Research Centre of Finland (VTT) as a research scientist among optical instrumentation, microsensing and biosensor applications. He has also worked as a research trainee and project research scientist in the Accelerator Laboratory of University of Jyväskylä (1996–1999).

Martin Albers holds a BSc in Analytical Chemistry (Leiderdorp, the Netherlands), MSc in Materials Chemistry (Tampere Technical University, Finland) and PhD in Biotechnology (Cranfield University, UK). He has worked in various subjects related to biosensors, such as antibody immobilization, design of functional coatings, surface modification of nanoparticles, optical properties of gold films and electrical conductivity of nanocomposites. He was employed at VTT, the Technical Research Centre of Finland as a Senior Scientist, and is presently working in the R&D section of BioNavis Ltd.

Matthijs J. van Lint studied chemistry at the Vrije Universiteit Amsterdam, where he obtained his MSc degree in 2012. Ensuing he pursued a PhD degree at the same University under the supervision of dr. Eelco Ruijter, dr. Rob J.M. van Spanning and prof. Romano Orru. During this time he worked on asymmetric syntheses of complex and biologically relevant natural products. His research interests include enzyme catalysis and multi-step total synthesis using epoxide chemistry.

Mr. Dick van Iperen is technical engineer at the Mechanical Workshop of the Faculty of Science at the Vrije Universiteit in Amsterdam. He is a specialist in the construction of (micro)fluidic parts for analytical-chemical purposes.

Jelmer J.A. Weda, research engineer at Vrije Universiteit Amsterdam obtained his engineering physics degree in 2008 from Technische Hogeschool Rijswijk (Bachelor of Engineering), with a minor in photonics. Prior to this position he worked as a research engineer at Academic Medical Center, Amsterdam (BMEP group). In 2011 he joined the biophotonics & medical imaging team at the physics department of the Vrije Universiteit Amsterdam, where the research focusses on optical coherence tomography and fluorescent imaging. In the last view year he gained experience in: optical system design, fiber optics, sample preparation, laser safety, medical device development and medical device compliance.

Dr. Johana Kuncová-Kallio, CEO at BioNavis Ltd has studied at Czech-Swiss Institute, at Czech Technical University in Prague (B.Sc. 1999), at University of Strathclyde (UK) and at Tampere University of Technology in Finland (M.Sc. 2002, Dr.Tech. 2007). She has been working as a researcher in the fields of instrumentation, point-of-care diagnostics, cell-based assays and established several courses in Microfluidics and Microsystems. She worked at Biosensing Competence Center and since 2011 she works in BioNavis Ltd, a company dedicated to expanding the capabilities of surface plasmon resonance in the fields of pharmaceutics, biosensing and material research.

Dr. Govert W. Somsen is professor of Biomolecular Analysis at Vrije Universiteit Amsterdam. He obtained his doctorate in Amsterdam, and subsequently was assistant and associate professor at the University of Groningen and Utrecht University. His current research interests include compositional and conformational characterization of intact biomacromolecules, bioactivity screening of compounds in complex samples, and metabolite analysis with particular attention for compound chirality. His group built an internationally recognized expertise in the hyphenation of capillary electrophoresis and liquid chromatography with mass spectrometry and optical spectroscopy for the detailed profiling of pharmaceutical proteins. Somsen is (co)author of over 145 peer-reviewed papers, and is editor of Journal of Chromatography B.

Dr. Jeroen Kool is an analytical chemist with research interests in high resolution screening of biologically active mixtures. His research achievements allow full compatibility of analytical separations with biological assays (including cellular) and parallel MS detection for investigation of bioactive mixtures (biopharmaceuticals, natural product extracts, metabolic mixtures, venoms, environmental mixtures) using miniaturized setups and nanospotting technologies. These techniques combining chromatography, mass spectrometry and bioassays in one analytical platform are now known as nanofractionation analytics. He also developed new technologies in the area of Surface Plasmon Resonance sensing.